The International Journal of Advanced Manufacturing Technology (2018) 95:2259–2268
https://doi.org/10.1007/s00170-017-1368-9

ORIGINAL ARTICLE

Model for surface topography prediction in mirror-milling of aircraft skin parts

Yan Bao[1] · Renke Kang[1] · Zhigang Dong[1,2] · Xianglong Zhu[1] · Changrui Wang[1] · Dongming Guo[1]

Received: 22 June 2017 / Accepted: 10 November 2017 / Published online: 22 November 2017

Abstract
As a new technology of aircraft skin processing, mirror-milling is an efficient and green processing technology, which is a gradually developmental substitute for chemical milling. The purpose of this research aims to study surface topography forming mechanism and the effect of support location on the surface topography forming in mirror-milling of aircraft skin parts. A new iterative workpiece deformation prediction model is proposed for mirror-milling error prediction of low-rigidity parts. In addition, the workpiece surface topographies are predicted and verified at different support locations. The results of the study are summarized: under the same processing parameters, the machined surface topographies with different characteristics are obtained only by changing the relative position between the support head and the milling head. The support location is the key parameter of reducing the workpiece deformation error.

Keywords Mirror milling · Surface topography · Support location · Aircraft skin

1 Introduction

Aircraft skin parts are important parts which constitute the aerodynamic configurations of aircrafts [1]. There are single curvature parts, double curvature parts, and even more complex shape parts among skin parts [2]. Sometimes the surface curvature is extremely variable over a whole part [3]. Lightweight design means less fuel consumption, which drives the aircraft technologist to focus on lightweight innovation [4]. So the skin parts need to be as thin as possible. Aircraft skin parts are characterized with large size, complex shape, thin-floor structure, and low rigidity [5–7].

Currently, the thinning tasks are accomplished by creating pockets in the skin panel by chemical machining [4]. Unfortunately, this chemical machining process ends with chemical pollutants to the environment. Most of the chemicals such as cleaning solutions, etchants, and strippers are very hazardous liquids. Specially, etchants are very harmful for workers safety [8]. Furthermore, due to the previous stage of stretching, most of the panel gets high variation of initial thickness. Besides, the material removal rate of chemical machining process is a constant. The above two reasons determine the fact that pocket floor thickness is irregular and imprecise [9, 10]. In addition, there is a long process cycle of aircraft thinning operation composed of several steps for different cutting depths, because chemical milling process is not capable of attaining different cutting depths in a single operation [11]. Also, a large amount of energy consumption is a bottleneck [12]. So, replacing this industrial chemical milling process with a lower emission and more environmentally friendly process is sought.

In order to address the above issues, mirror-milling system (MMS) is proposed to machine aircraft skins and now used in Airbus Company [13, 14]. This system contains two independent five axis machines on opposite sides of the same skin part moving in a coordinated manner. The first one performs the pocket machining, while the other provides the support on the opposite side. The support which must withstand the thrust force from the milling operation also needs to move smoothly with low frictional force, which is usually a metallic sphere [4, 10, 15, 16].Compared its superiorities with chemical milling, MMS has a potential to become the next-generation processing technology of aircraft skin [12].

As a new technology of reducing the thickness of thin and large aircraft skin parts, MMS have been widely emerging in

✉ Zhigang Dong
dongzg@dlut.edu.cn

[1] Key Laboratory for Precision and Non-traditional Machining Technology of Ministry of Education, Dalian University of Technology, Dalian 116024, People's Republic of China

[2] Institute of Advanced Manufacturing Technology, Dalian University of Technology, Dalian 116024, People's Republic of China

practical applications. A mass of researches have been presented. Mahmud at University of Montreal proposes a process for aircraft skin milling with a magnetic grasping and machining end effector [4]. The machining end effector is moved by a manipulator, while the sliding magnetic grasping mechanism holds the skin part to counteract the thrust force generated by the milling process. By this way, only one set of multi-axis equipment is needed to complete the mirror-milling process, which greatly reduces the equipment cost. A milling force model considering the influence of the spindle angle is established in order to determine the minimum clamping force, and a master-to-slave motion transfer function is proposed by only considering the lateral sliding motion [17, 18]. However, the processing result is limited by immature process and equipment status. Li and his team propose a feature-based fitting module for broken surfaces of complex aircraft skin parts by mirror-milling. The process information is associated with geometric information based on features, and then the machining surface and its corresponding tool path are extracted automatically [3, 19, 20]. A stiffness model for a mirror-milling device is established by Wang et al. The distribution of the synthetic stiffness is obtained and optimized by adding a redundant actuation [21, 22]. Xiao and his team propose another kind of mirror-milling system which consists of milling head, workpiece fixture unit, and two support heads. During the manufacturing, these two support heads are periodically repositioned by the way of vacuum absorption to support the thin workpiece, so that the deformation and suppress vibration of workpiece can be reduced. A method for the planning of support head moving path under a given cutting path is developed [23–25]. However, this system is not the same as the previously mentioned MMS in mechanism, because the two support heads cannot move continuously but in a path constituted by limited position points. Bao at Dalian University of Technology proposes a milling force model for mirror-milling of aircraft skin. A new support method used in MMS can eliminate the aircraft skin surface scratches caused by rolling support or sliding support. The effects of thickness and stiffness of liquid film on surface quality and dimensional uniformity of workpiece are analyzed [26, 27]. Although a great progress has been made in recent years, it is still difficult to reach the ideal machining precision due to the bad rigidity and weak intensity [25]. Aircraft skin parts are very easily distorted when being machined, bad surface finish or even marks appear on the final surface when machining parameters are selected improperly [28, 29]. The accuracy of the surface topography is one of the key factors for achieving the required dimensional and geometric tolerances, and it plays a

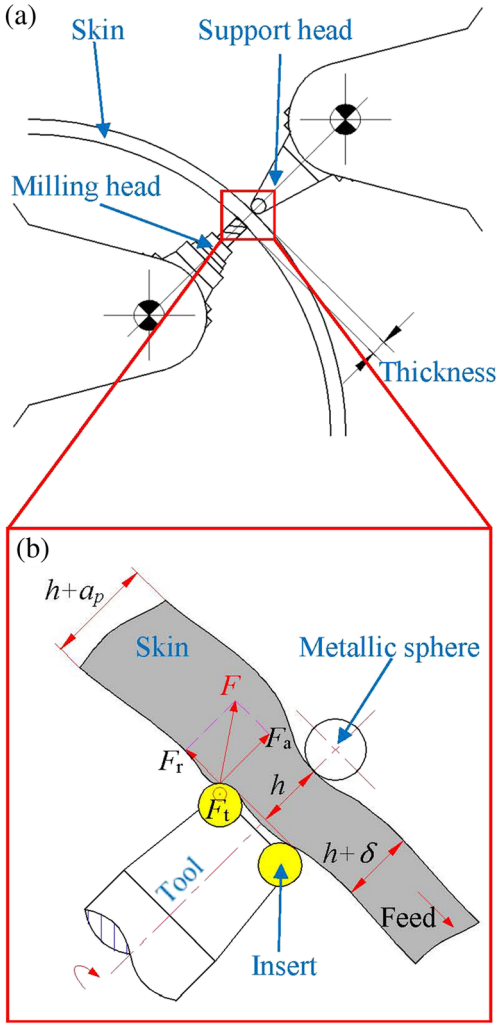

Fig. 1 **a** Mirror-milling setup of aircraft skin with MMS. **b** Schematic diagram of cutting zone in MMS

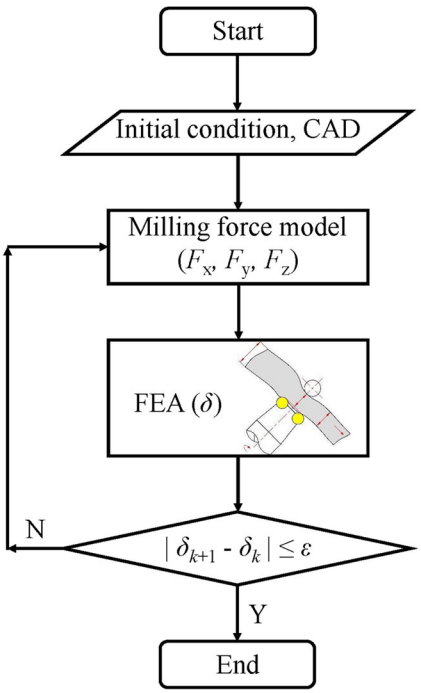

Fig. 2 Flowchart for an iterative workpiece deformation prediction model

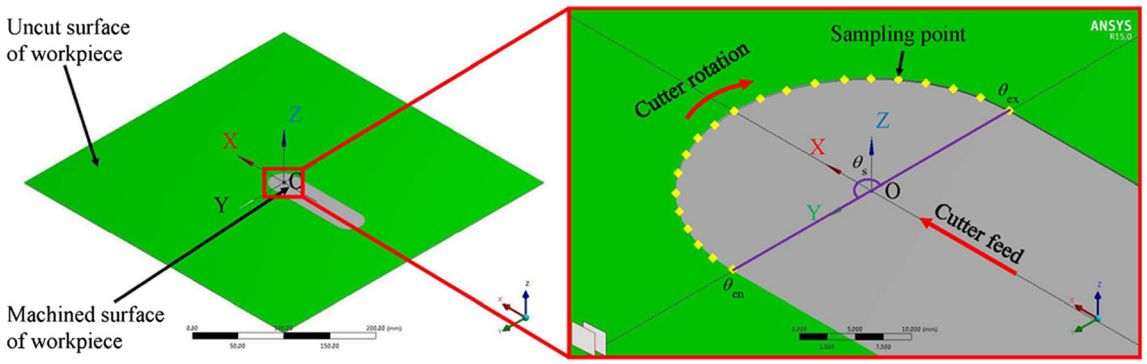

Fig. 3 Schematic of cutting zone for FEA modeling

significant role in ensuring the overall product quality, because it is often directly related to the product's functional performance. The workpiece topography error is greatly affected by the support location of MMS [30]. However, little literature has been published on surface topography forming mechanism in mirror-milling of aircraft skin parts. Therefore, it is essential to study how the support location affects the surface topography forming.

The paper focuses on the model of workpiece deformation for mirror-milling error prediction of low-rigidity parts. The effect of support location on the surface topography forming in mirror-milling of aircraft skin parts is also studied. The remainder of the paper is organized as follows: in Section 2, an iterative workpiece deformation prediction model is proposed; modeling of workpiece surface topography in mirror-milling is presented in Section 3; the predicted and experimental results of surface topography at different support locations are discussed in Section 4; and the final conclusions are drawn in Section 5.

2 Prediction of workpiece deformation

During mirror-milling of aircraft skin parts, the milling head and the support head are on the same vector along the normal direction of the workpiece, so the distance between two heads is equal to the machined skin thickness (Fig. 1a) [2]. However, the rigidity of the workpiece is low in tool axial direction in which the workpiece deformation is easier to produce, and the axial force also will be affected by the deformation of the workpiece in turn (Fig. 1b). The workpiece surface topography error is mainly induced by the tool axial deformation; thus, the deformation of workpiece in tool axial direction is the only reference parameter in this paper.

2.1 Deformation prediction methodology

Mirror milling of aircraft skin parts is a typical process of low-rigidity workpiece milling. The cutting forces depend on the chip thickness and contact length which is a function of the axial cutting depth, at the same time, the axial cutting depth is another function of the workpiece deformation impacted by the cutting forces [31, 32]. To resolve this complex dependency, an interactive approach is employed to find the equilibrium state of the cutting force and workpiece deformation [33–35]. The iterative workpiece deformation prediction model is outlined in Fig. 2. The milling force, F, and workpiece deformation, δ, negotiate, so the workpiece deformation eventually converges to a value within a given tolerance, ε, in successive iterative steps $(k+1)$ and k:

$$|\delta_{k+1}-\delta_k| \le \varepsilon \tag{1}$$

2.2 Milling force model

An enormous amount of researches have been carried out on modeling of milling force, which can be roughly divided into four categories: empirical model, analytical model, mechanistic model, and numerical model [36–43]. Among them, the mechanistic model has been widely implemented with the advantages of less experimental work and better accuracy for prediction [30]. The mechanistic model combines three steps [44]: first, calculation of the position of each discretized cutting edge; second, corresponding cutting depth associated; and third, total of all the elementary forces. At each discretized

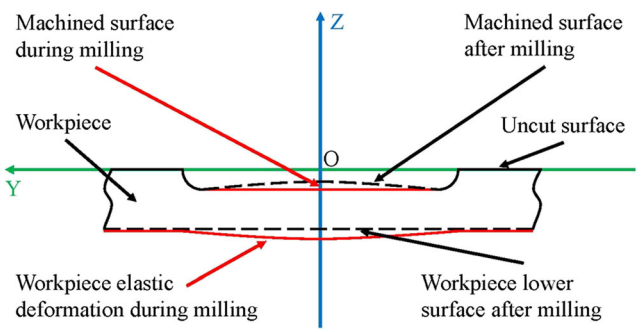

Fig. 4 Section view in plane OYZ

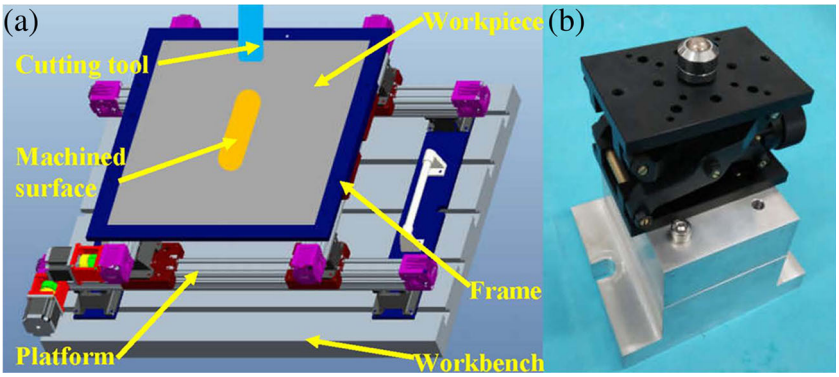

Fig. 5 Experimental platform. **a** Two-dimensional horizontal moving platform. **b** Supporting device

cutting edge, the following cutting law has been applied for tangential, radial, and axial forces [31]:

$$\begin{aligned} dF_t &= K_{te}dS + K_{tc}h\,dz \\ dF_r &= K_{re}dS + K_{rc}h\,dz \\ dF_a &= K_{ae}dS + K_{ac}h\,dz \end{aligned} \tag{2}$$

with dS the elementary length of the cutting edge, h the uncut chip thickness, and dz. the elementary height of the cutting edge. Parameters K_{te}, K_{re}, K_{ae}, K_{tc}, K_{rc}, and K_{ac} are referred to as the milling force coefficients, which are experimentally determined. After coordinate transformation and integration, the total milling forces can be obtained. The influences of milling speed and tool wear on milling forces are reported in previous work [30].

2.3 Finite element analysis

For simplification, the aircraft skin part is assumed to be a square aluminum plate with side length 400 mm and thickness 1 mm (Fig. 3). The Young's Modulus of the aluminum alloy is 71 GPa, and the Poisson's ratio is 0.33. The required machined topography is a flat surface parallel to the upper surface (plane OXY). During the milling process, the workpiece deformation in direction Z is perpendicular to the machined surface and has the most significant impact on forming the surface topography error. The contributions of the workpiece deformations in X and Y directions can be negligible. Therefore, this investigation only focused on the error prediction in Z direction.

The slot milling process is applied to the workpiece under the conditions of milling speed 325 m/min, feed per tooth 0.12 mm, and axial cutting depth 0.2 mm, and the predicted milling force [30] is used for FEA. The support head was simplified to a steel ball. The Young's Modulus of the steel is 200 GPa, and Poisson's ratio is 0.3. All the four sides of the workpiece and the steel ball are fixed. In MMS, the milling head and support head are on the same vector along the normal direction of the workpiece. However, the supported area is smaller than the milling area, which can result in workpiece elastic deformation during milling. The milling forces are variable in the direction of the milling tool axis, which may also produce different workpiece deformation along Y direction (Fig. 4).The cutter sweep angle ($\theta_s = \theta_{ex} - \theta_{en}$) was divided into 20 parts, where θ_{ex} is exit angle and θ_{en} is entrance angle. In the continuous cutting cycle, 21 points were taken as sampling point at the same intervals. An instantaneous milling force was applied to each point corresponding to a sweep angle. An FEA model of the aluminum plate is developed. As long as the deformation of the workpiece under each force is calculated separately, the deformation of the workpiece in the whole process can be fitted.

2.4 Iterative workpiece deformation simulation and verification

In order to study the machining mechanism and the deformation of the workpiece, an experimental setup was constructed. In MMS, the milling and support heads during machining are on the same vector along the normal direction of the aircraft skin. In the experiment setup, a two-dimensional horizontal

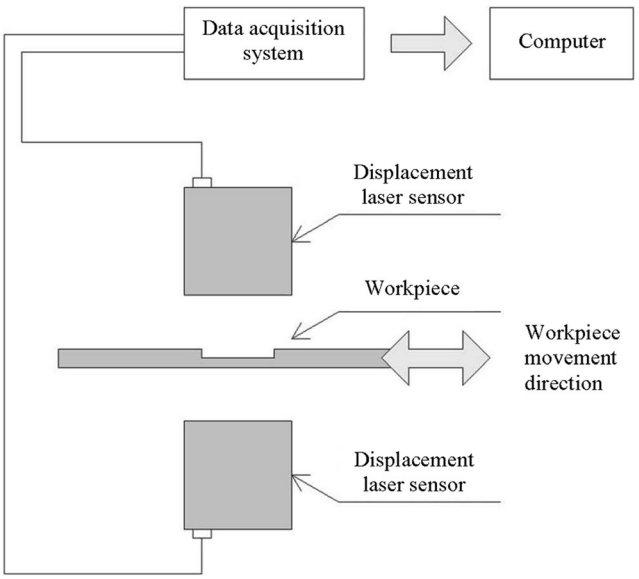

Fig. 6 Thickness measurement device with two laser displacement sensors

Table 1 Predicted workpiece deformation after multi-level iteration

θ (degree)	δ_0 (μm)	Accuracy (%)	δ_1 (μm)	Accuracy (%)	δ_2 (μm)	Accuracy (%)	δ_k (μm)
0	47.7	76.1	36.3	94.3	39.0	98.7	38.5
9	59.1	70.7	41.6	91.0	46.8	97.6	45.7
18	70.9	65.2	45.8	87.1	54.7	96.0	52.6
27	83.0	58.8	48.6	82.7	62.8	93.2	58.8
36	95.4	53.0	49.9	76.9	71.6	89.7	64.9
45	107.3	46.9	49.7	70.9	80.6	85.0	70.1
54	117.7	42.4	48.4	64.8	89.2	80.6	74.7
63	126.5	37.8	46.5	59.6	97.1	75.5	78.0
72	133.0	34.2	44.6	55.6	103.6	70.8	80.2
81	137.0	32.7	43.1	52.6	107.5	68.7	81.9
90	138.7	32.1	42.5	51.5	109.2	67.8	82.6
99	137.0	32.7	43.1	52.6	107.5	68.7	81.9
108	133.0	34.2	44.6	55.6	103.6	70.8	80.2
117	126.5	37.8	46.5	59.6	97.1	75.5	78.0
126	117.7	42.4	48.4	64.8	89.2	80.6	74.7
135	107.3	46.9	49.7	70.9	80.6	85.0	70.1
144	95.4	53.0	49.9	76.9	71.6	89.7	64.9
153	83.0	58.8	48.6	82.7	62.8	93.2	58.8
162	70.9	65.2	45.8	87.1	54.7	96.0	52.6
171	59.1	70.7	41.6	91.0	46.8	97.6	45.7
180	47.7	76.1	36.3	94.3	39.0	98.7	38.5
Average		50.9		72.5		84.7	
Std.		29.4		20.3		13.0	

moving platform (Fig. 5a) and a support device (Fig. 5b) were installed on the workbench of a three-axis vertical machine tool. The support device was composed of a lifting platform and a ball bearing mounted on the platform. The workpiece was clamped on a large frame which was mounted on the two-dimensional horizontal moving platform. During machining, the axis of the cutting tool and the support device were on the same vector, and the cutting tool was fed to a limited distance (the designed thickness of the skin). The feed motion was realized by the movement of the workpiece. The workpiece material used is aluminum alloy 7075. A DEREK TP-C25-35-160-2 T abandon right-angle cutter with 35 mm diameter and 7° helix angle was applied, on which a TPMN160308-UTi20T cemented carbide inserts from Mitsubishi was fixed. The slot milling experiment was conducted under the conditions of milling speed 325 m/min, feed per tooth 0.12 mm, and axial cutting depth 0.2 mm.

The workpiece is clamped on a large frame, so the workpiece rigidity varies in different positions, resulting in the workpiece produces different deformation in different positions under the same cutting parameters. Thus, only the deformation of the workpiece center was measured for comparision (Fig. 5a). After milling, the actual thickness of the workpiece was measured by two displacement laser sensors (Keyence, LK-H025), which were placed face to face in the opposite directions (Fig. 6). During measuring, the two displacement laser sensors are fixed, while the workpiece is moved horizontally by the two-dimensional horizontal moving platform. The thickness changes of the workpiece can be obtained by adding the data measured by the two sensors. The error convergence tolerance, ε, in workpiece deformation prediction (Fig. 2) is set as 1%.

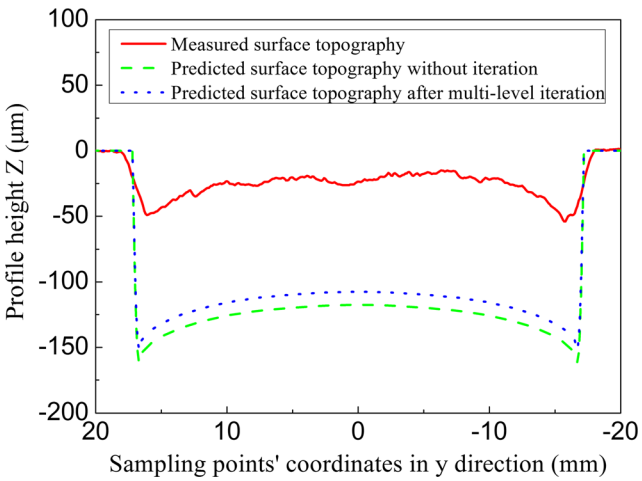

Fig. 7 Predicted and measured surface topographies of the 400 × 400 × 1 workpiece

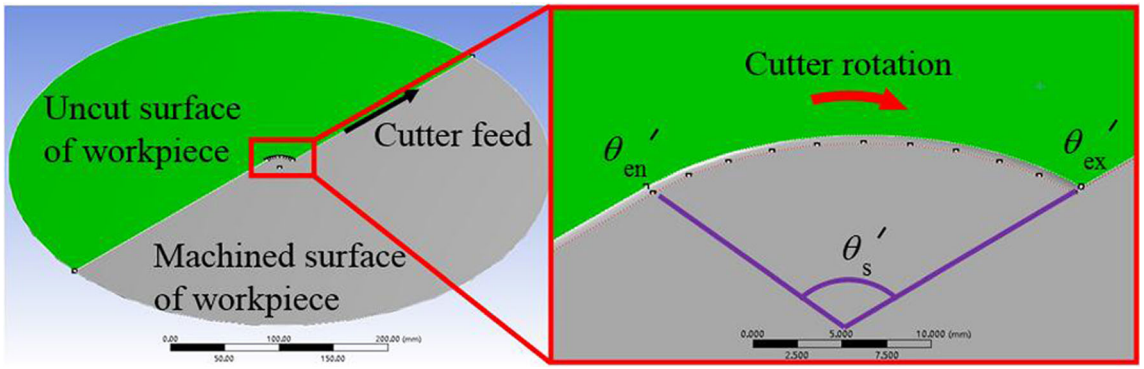

Fig. 8 Schematic of cutting zone for the FEA model of mirror-milling the skin panel

The predicted workpiece deformation values are used for all subsequent iterations, which are listed in Table 1. The first column (θ) represents the angles (measured counterclockwise from the entrance angle, θ_{en}) of the sampling points along the cutting tool trajectory. The predicted values without iteration, δ_0, after the single-level, δ_1, second-level, δ_2, and multi-level, δ_k, iteration are shown respectively in column 2, column 4, column 6, and column 8. The predicted values from different levels illustrate the convergence of the iterative prediction plan. Columns 3, 5, and 7 show the percentage of the predicted values in each level compared to the final converged results. Table 1 shows that in 0-level (initial level) deformation prediction, it can capture over 50.9% of total amount of deformation with the standard deviation of about 29.4%. The first-level error prediction can capture up to 72.5% of total amount of error with the standard deviation of about 20.3%, while the third-level error prediction can capture up to 84.7% of total amount of error with the standard deviation of about 13.0%. The results listed in Table 1 clearly indicate that the convergence of the proposed error prediction plan is robust. It can be concluded that the convergence is slow when the milling force is large. In other words, at 0° and 180°, the number of iterations is smaller than that at 90° to achieve the target error convergence tolerance, ε.

The predicted and the measured workpiece surface topographies are shown in Fig. 7. The height of the workpiece upper surface is set to zero, so the material removal is marked as the negative profile height (Z). The fluctuation rule of the three profile curves is consistent, that is, when the cutting force is large, the workpiece deformation is large, but the actual cutting depth is small. Compared with the predicted surface topography without iteration, after multi-level iteration, the predicted one is closer to the measured one. The difference between the predicted and the measured surface topographies is caused by the different fixture methods. In the experiment, the method of fixing the workpiece is not as ideal as that in FEA, which leads to greater workpiece deformation and smaller cutting depth.

3 Modeling of workpiece surface topography in mirror-milling

In MMS, the workpiece surface topography is greatly affected by the workpiece elastic deformation. Therefore, it is essential to study how the support location affects the surface topography forming. Whether the array suction cups or the surrounding holders, as flexible fixtures, are used to fix the periphery of the workpiece, which is far away from the work region, the distance between the fixed point and the support point is much larger than that between the cutting force point and the support point [10, 45]. Thus, in the finite element simulation, some system assumptions are set as follows:

1. The workpiece material is completely isotropic and linearly elastic, and its physical properties have no change during the milling process;
2. The instantaneous deformation of the workpiece during the machining process is in the elastic range;
3. The instantaneous deformation of the workpiece by the machining process and the elastic springback after the machining process are the same in magnitude but opposite in directions;

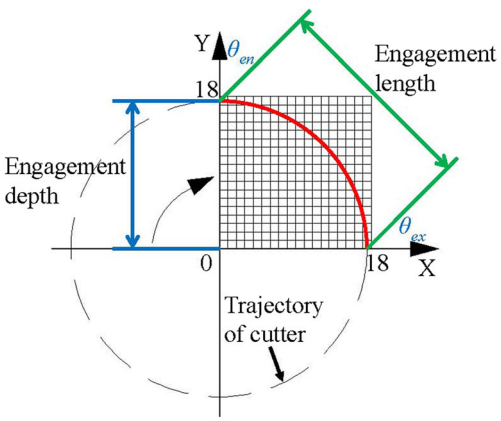

Fig. 9 Supporting locations in the FEM calculation

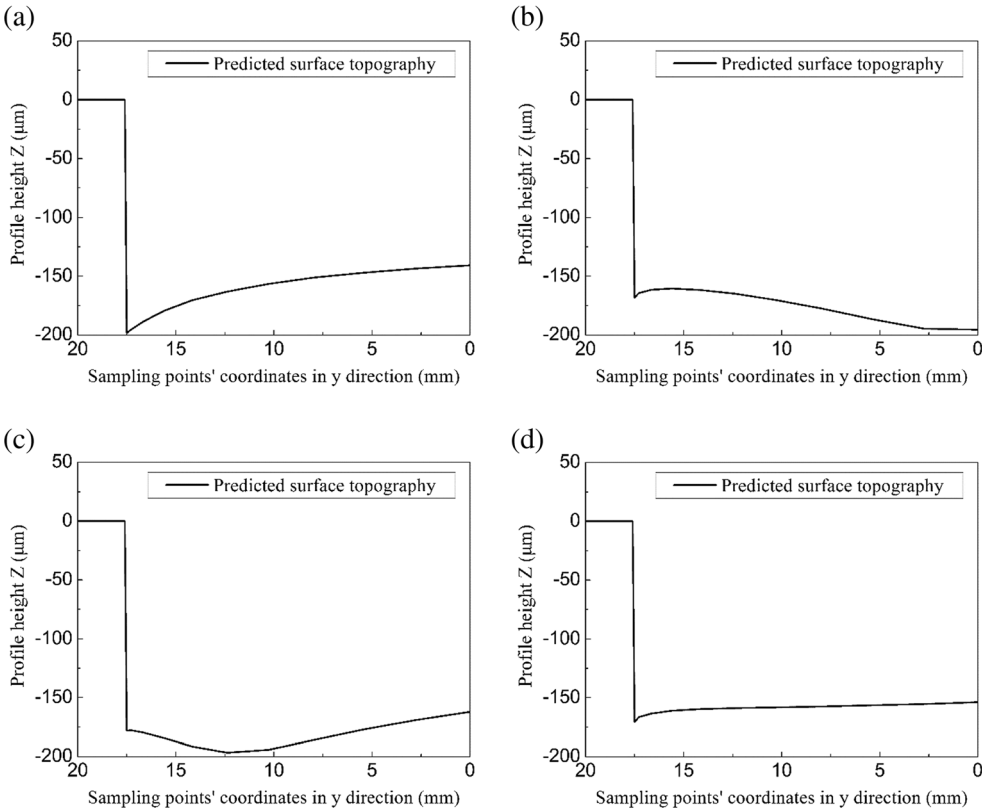

Fig. 10 Predicted surface topographies of workpiece at some representative support locations. **a** Support location A ($x = 0$, $y = 16$). **b** Support location B ($x = 16$, $y = 1$). **c** Support location C ($x = 14$, $y = 15$). **d** Support location D ($x = 6$, $y = 2$)

4. The effect of the distance between different fixed points and the support point on the deformation of the workpiece are negligible;
5. The deformations of the workpiece produced by residual stress, vibration, and tool installation error are negligible.

Based on the above assumptions, a 500-mm diameter circular 7075 aluminum alloy plate was used in the FEA modeling (Fig. 8). In the case of finish machining, the initial skin thickness 1 mm, the axial cutting depth 0.2 mm, and the radial cutting depth 17.5 mm (cutter half immersion), and the predicted milling forces were used for FEA. The support head was simplified to a steel ball with the same diameter. Both the periphery of the workpiece and the steel ball were fixed. The cutter sweep angle ($\theta_s' = \theta_{ex}' - \theta_{en}'$) was divided into 10 parts, where θ_{ex}' is exit angle and θ_{en}' is entrance angle. An instantaneous milling force was applied to each point corresponding to a sweep angle. An FEA model of the mirror-milling skin panel was developed.

4 Results and discussion

From the simulation results of workpiece deformation, it is known that the deformation gradually varies with the milling force. The machining area is simulated using FEM in order to study the surface topography forming mechanism and reduce the workpiece deformation by optimizing the support location. In the directions of the entrance point and the exit point from the original support point, 18 equal parts are taken with 1×1 mm^2 per part, and the matrix of support location is established and shown in Fig. 9. The deformation of the work

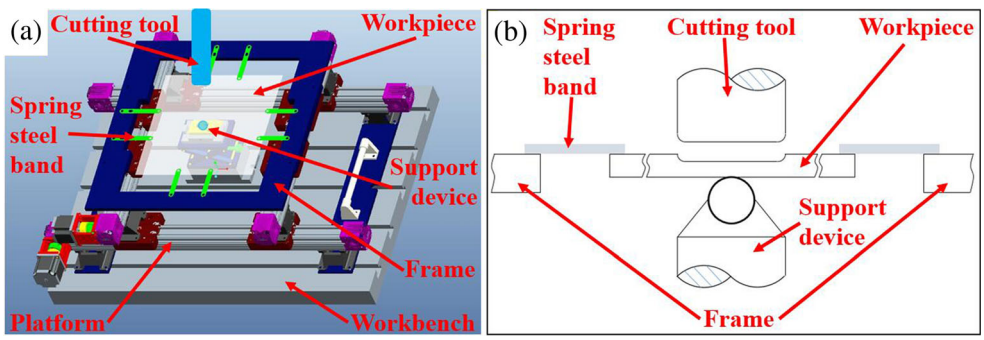

Fig. 11 **a** Schematic diagram of experimental setup. **b** Section view of experimental setup

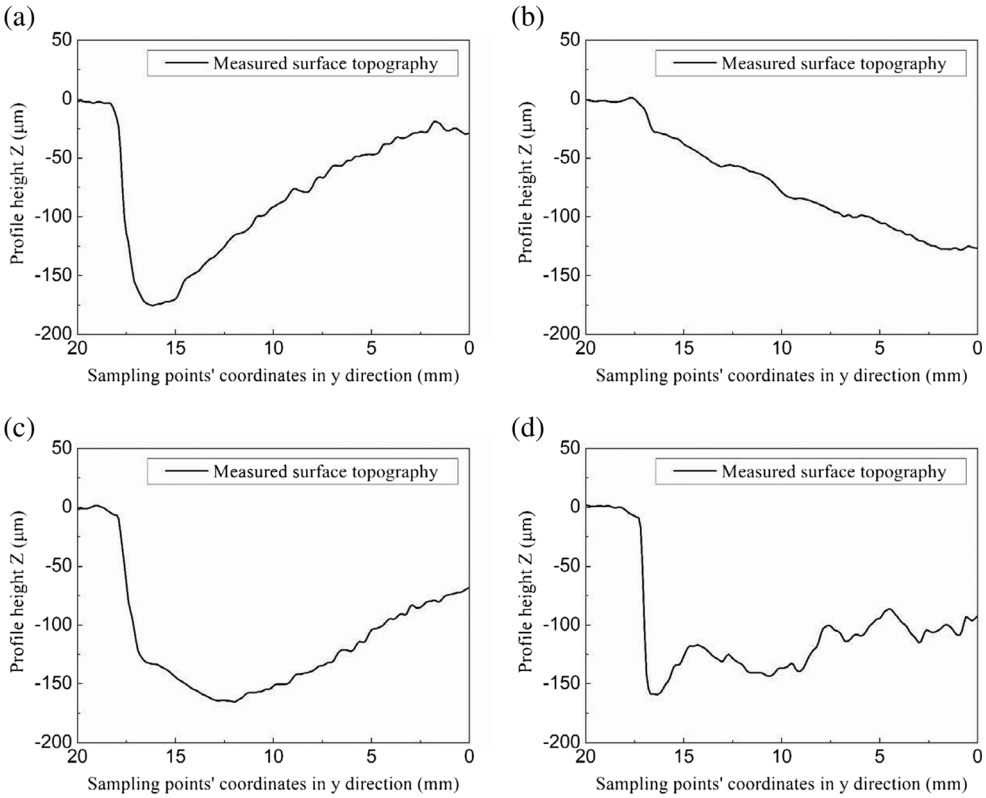

Fig. 12 Measured surface topographies of workpiece at the support locations. **a** Support location A ($x = 0$, $y = 16$). **b** Support location B ($x = 16$, $y = 1$). **c** Support location C ($x = 14$, $y = 15$). **d** Support location D ($x = 6$, $y = 2$)

area is calculated by FEM at every support location. Figure 10 shows some representative results.

As shown in Fig. 10a, when the support head is mounted at point A ($x = 0$, $y = 16$), from cut-in to cut-out, the workpiece deformation increases gradually. However, the deformation tendency of workpiece is just the opposite at support location B ($x = 16$, $y = 1$). This is because the workpiece near the support head is high in rigidity, which leads little deformation. At support location A, the increment of workpiece profile height is greater than the decrement of that at support location B. The reason is that the cutting force increases gradually from cut-in to cut-out; the lowest rigidity point of workpiece A is near cut-out point, but that of workpiece B is near cut-out point. Besides, at support location C ($x = 14$, $y = 15$), the profile height increases after an initial decrease; the deformation fluctuation is much smaller at location D ($x = 6$, $y = 2$) compared with the others. By analyzing the simulation results, flat surface topographies can be obtained by changing the support head location, making the rigidity distribution of the workpiece in the machining area consistent with the variation of the milling force.

In order to verify the predicted workpiece surface topographies, a set of experiments was designed. In order to reduce the difference of rigidity distribution and simulate the real condition of mirror-milling low-rigidity workpiece, the experimental platform (Fig. 5) was changed slightly. A 300 × 300 × 1 workpiece was fixed onto the frame by eight spring steel bands (Fig. 11).

Although the fixture methods of the workpiece are different in the experiment and MMS, the deformation rules for the middle work area of the workpiece in both the experiment and MMS are the same, resulting in little difference in deformation. The verification experiment was performed. The measured surface topographies of workpiece at different support locations are shown in Fig. 12.

Comparing the predicted (Fig. 10) and measured (Fig. 12) results, it indicates that they are in a good agreement not only in shape but also in magnitude. The simulation system meets the anticipated request. The deformation fluctuation at support location D ($x = 6$, $y = 2$) is less than the others, which means the thickness uniformity of the workpiece is better. The measured profile height difference of workpiece A is 156.475 μm, while that of workpiece D is 73 μm. That is to say, compared with the deformation fluctuation due to the support at location A, that at location D is decreased by 53.35%.

5 Conclusions

This study proposes a new iterative workpiece deformation prediction model suitable for mirror-milling error prediction of low-rigidity parts, which is verified by the experiment. In addition, the model for surface topography prediction in mirror-milling matches to the anticipated request. The results show that flat surface topographies can be obtained by changing the support head location, making the rigidity distribution

of the workpiece in the machining area consistent with the variation of the milling force. The profile height difference of workpiece is decreased.

Acknowledgements This work was supported by the National Natural Science Foundation of China [grant number 51575085]; the Science Fund for Creative Research Groups of NSFC [grant number 51321004]; and the National Engineering and Research Center for Commercial Aircraft Manufacturing [grant number 201500308].

Compliance with ethical standards

Conflict of interest The authors declare that they have no conflict of interest.

References

1. Zhu X, Xiang B, Wang Y, Li Y (2015) Application and research of mirror milling technology for aircraft skin. Trainer 2:23–27
2. Zhang T (2011) Up-to-date technology for precision machining of aircraft skin thickness—greenhouse machining technology for the CNC milling instead of chemical milling. Trainer 4:25–29
3. Zhou G, Li Y, Liu C, Hao X (2016) A feature-based automatic broken surfaces fitting method for complex aircraft skin parts. Int J Adv Manuf Technol 84(5):1001–1011. https://doi.org/10.1007/s00170-015-7774-y
4. Mahmud A (2015) Mechanical pocket milling of thin aluminum panel with a grasping and machining end effector. Universite De Montreal, Dissertation
5. Han Z, Dai L, Zhang L (2009) Current status of large aircraft skin and panel manufacturing technologies. Aeronaut Manuf Technol 4:64–66. https://doi.org/10.3969/j.issn.1671-833X.2009.04.007
6. Zhou K (2012) Flexible tooling and fixture technology of large thin-wall part manufacturing for aircraft. Aeronaut Manuf Technol 3:34–39. https://doi.org/10.3969/j.issn.1671-833X.2012.03.003
7. Herranz S, Campa FJ, Lopez de Lacalle LN, Rivero A, Lamikiz A, Ukar E, Sanchez JA, Bravo U (2005) The milling of airframe components with low rigidity: a general approach to avoid static and dynamic problems. Proc Inst Mech Eng B J Eng Manuf 219(11):789–801. https://doi.org/10.1243/095440505X32742
8. Cakir O, Yardimeden A, Ozben T (2007) Chemical machining. Arch. Mater Sci Eng 28(8):499–502
9. Lin C, Cai J, Zeng F, Huang X, Du N, Zhao Q (2010) Chemical milling technology and influencing factors of processing quality of LY12 aluminum alloy. Fail Anal Prev 5(1):8–12, 16. https://doi.org/10.3969/j.issn.1673-6214.2010.01.003
10. Panczuk R, Foissac PY (2010) Process and a device for the machining of panels. US patent, 7682112 B2
11. Jin Y (2009) Design of equipment for chemical milling of rocket tank sheets. Missile Space Vehcile 2:52–56. https://doi.org/10.3969/j.issn.1004-7182.2009.02.013
12. Lu D (2010) New generation green machining technology for aircraft skin. Aeronaut Manuf Technol 16:102–103. https://doi.org/10.3969/j.issn.1671-833X.2010.16.024
13. Zhang Z, Xu X (2010) MMS: the latest green skin machining system. Aeronaut Manuf Technol 19:84–86. https://doi.org/10.3969/j.issn.1671-833X.2010.19.011
14. Zhang X, Duan X (2015) Flexible champing and CNC milling technology of aircraft skin. Aeronaut Manuf Technol (S1): 42–44. https://doi.org/10.16080/j.issn1671-833x.2015.S1.042
15. Xu M, Xiang B, Li X, Wang Y, Lan H (2014) Application of mirror milling system and advanced machining technology for aircraft skin. Manuf Technol Mach Tool 11:40–43. https://doi.org/10.3969/j.issn.1005-2402.2014.11.016
16. Xiang B, Huang J, Xu J, Zhou X, Li Y, Hao X (2015) Mirror top bracing technology in milling aircraft skin. Manuf Technol Mach Tool 4:92–96. https://doi.org/10.3969/j.issn.1005-2402.2015.04.023
17. Mahmud A, Mayer JRR, Baron L (2015) Determining the minimum clamping force by cutting force simulation in aerospace fuselage pocket machining. Int J Adv Manuf Technol 80(9):1751–1758. https://doi.org/10.1007/s00170-015-7104-4
18. Mahmud A, Mayer JRR, Baron L (2015) Magnetic attraction forces between permanent magnet group arrays in a mobile magnetic clamp for pocket machining. CIRP J Manuf Sci Technol 11:82–88. https://doi.org/10.1016/j.cirpj.2015.08.005
19. Liu S, Li Y, Hao X, Liu C, Xiang B (2016) Feature-based uncut region tool path optimization method for skin parts machined by mirror milling system. Acta Aeronautica et Astronautica Sincia 37(7):2295–2302. https://doi.org/10.7527/S1000-6893.2015.0240
20. Hu M, Xiang B, Li Y, Xu M, Zhu X (2016) Application of feature-based rapid programming technology for aircraft panels. Manuf Technol Mach Tool 1:148–152. https://doi.org/10.3969/j.issn.1005-2402.2016.01.041
21. Hao J, Zhao Y, Wang H, Sheng D (2015) Synthetical stiffness analysis and optimization of mirror support mechanism for thin-walled structures. Mach Des Res 31(2):155–159 **163**
22. Zhao Y, Wang Z, Wang H, Hao J, Yu D (2015) Stiffness analysis and optimization of supporting mechanism based on tricept for thin-walled part milling system. The 14th IFToMM World Congress, Taipei, Taiwan, 25-30 October 2015. https://doi.org/10.6567/IFToMM.14TH.WC.OS13.075
23. Xiao J, Yao Y, Huang T, Lin B, Ji J, Zhang X, Lin B (2016) Hard-soft multipoint follow-up support head used for image processing. China patent, 14668989B
24. Xiao J, Yao Y, Huang T, Lin B, Ji J (2017) Sucking support head provided with rigid and flexible supports and used for machining grids of thin-walled workpiece. China patent, 104690577B
25. Lan J, Lin B, Huang T, Xiao J, Zhang X, Fei J (2016) Path planning for support heads in mirror-milling machining system. Int J Adv Manuf Technol (in press) 91(1-4):1–12. https://doi.org/10.1007/s00170-016-9725-7
26. Bao Y, Dong Z, Kang R, Li Z, Yuan Y (2016) Milling force and machining deformation in mirror milling of aircraft skin. Adv Mater Res 1136:149–155. https://doi.org/10.4028/www.scientific.net/AMR.1136.149
27. Li Z, Bao Y, Kang R, Dong Z, Zhou P, Jin Z (2016) An advanced support method of aircraft skin mirror milling—fluid lubricating support. Mater Sci Forum 874:469–474. https://doi.org/10.4028/www.scientific.net/MSF.874.469
28. Campa FJ, Lopez de Lacalle LN, Celaya A (2011) Chatter avoidance in the milling of thin floors with bull-nose end mills: model and stability diagrams. Int J Mach Tools Manuf 51(1):43–53. https://doi.org/10.1016/j.ijmachtools.2010.09.008
29. Mundim RB, Borille AV (2017) An approach for reducing undesired vibrations in milling of low rigidity structures. Int J Adv Manuf Technol 88(1–4):971–983. https://doi.org/10.1007/s00170-016-8804-0
30. Bao Y, Zhu X, Kang R, Dong Z, Zhang B, Guo D (2016, in press) Optimization of support location in mirror-milling of aircraft skins. Proc Inst Mech Eng B J Eng Manuf:1–8. https://doi.org/10.1177/0954405416673110
31. Budak E, Altintas Y, Armarego EJA (1996) Prediction of milling force coefficients from orthogonal cutting data. Trans ASME, J Manuf Sci Eng 118(2):216–224. https://doi.org/10.1115/1.2831014
32. Budak E, Altintas Y (1995) Modeling and avoidance of static form errors in peripheral milling of plates. Int J Mach Tools Manuf 35(3):459–476. https://doi.org/10.1016/0890-6955(94)P2628-S

33. Ratchev S, Liu S, Huang W, Becher AA (2004) A flexible force model for end milling of low-rigidity parts. J Mater Process Technol 153-154:134–138. https://doi.org/10.1016/j.jmatprotec.2004.04.300
34. Ratchev S, Liu S, Huang W, Becher AA (2006) An advanced FEA based force induced error compensation strategy in milling. Int J Mach Tools Manuf 46(5):542–551. https://doi.org/10.1016/j.ijmachtools.2005.06.003
35. Ratchev S, Liu S, Huang W, Becher AA (2004) Milling error prediction and compensation in machining of low-rigidity parts. Int J Mach Tools Manuf 44(15):1629–1641. https://doi.org/10.1016/j.ijmachtools.2004.06.001
36. Altintas Y (2012) Manufacturing automation: metal cutting mechanics, machine tool vibrations, and CNC design, 2nd edn. Cambridge University Press, New York
37. Nakayama K, Arai M, Takei K (1983) Semi-empirical equations for three components of resultant cutting force. CIRP Ann Manuf Technol 32(1):33–35. https://doi.org/10.1016/S0007-8506(07)63356-3
38. Brown CA, Von Turkovich BF (1983) A practical method for estimating machining forces from tool-chip contact area. CIRP Ann Manuf Technol 32(1):91–93. https://doi.org/10.1016/S0007-8506(07)63368-X
39. Oxley PLB (1989) Mechanics of machining: an analytical approach to assessing machinability. Ellis Horwood, Chichester
40. Lee P, Altinas Y (1996) Prediction of ball-end milling forces from orthogonal cutting data. Int J Mach Tools Manuf 36(9):1059–1072. https://doi.org/10.1016/0890-6955(95)00081-X
41. Movahhedy M, Gadala MS, Altintas Y (2000) Simulation of the orthogonal metal cutting process using an arbitrary Lagrangian-Eulerian finite-element method. J Mater Process Technol 103(2):267–275. https://doi.org/10.1016/S0924-0136(00)00480-5
42. Limido J, Espinosa C, Salauna M, Lacome JL (2007) SPH method applied to high speed cutting modelling. Int J Mech Sci 49(7):898–908. https://doi.org/10.1016/j.ijmecsci.2006.11.005
43. Jin X, Altintas Y (2011) Slip-line field model of micro-cutting process with round tool edge effect. J Mater Process Technol 211(3):339–355. https://doi.org/10.1016/j.jmatprotec.2010.10.006
44. Arnaud L, Gonzalo O, Seguy S, Jauregi H, Peigne G (2011) Simulation of low rigidity part machining applied to thin-walled structures. Int J Adv Manuf Technol 54(5–8):479–488. https://doi.org/10.1007/s00170-010-2976-9
45. Martinez MT, Fuerte SE (1992) Machine tool installation for supporting and machining workpieces. US patent 5163793